Serotonergic and dopaminergic neurons in the dorsal raphe are differentially altered in a mouse model for parkinsonism.

Laura Boi[1†], Yvonne Johansson[1,2†], Raffaella Tonini[3], Rosario Moratalla[4,5], Gilberto Fisone[1‡]*, Gilad Silberberg[1‡]*.

1 Department of Neuroscience, Karolinska Institutet, Stockholm 17177, Sweden.
2 Sainsbury Wellcome Centre for Neural Circuits and Behaviour, University College London, London, UK.
3 Neuromodulation of Cortical and Subcortical Circuits Laboratory, Istituto Italiano di Tecnologia, Genova, Italy.
4 Cajal Institute, Spanish National Research Council (CSIC), Madrid, Spain.
5 CIBERNED, Instituto de Salud Carlos III, Madrid, Spain.

† These authors contributed equally to this work
‡ These authors contributed equally to this work
* Corresponding author

Abstract

Parkinson's disease (PD) is characterized by motor impairments caused by degeneration of dopamine neurons in the substantia nigra pars compacta. In addition to these symptoms, PD patients often suffer from non-motor co-morbidities including sleep and psychiatric disturbances, which are thought to depend on concomitant alterations of serotonergic and noradrenergic transmission. A primary locus of serotonergic neurons is the dorsal raphe nucleus (DRN), providing brain-wide serotonergic input. Here, we identified electrophysiological and morphological parameters to classify serotonergic and dopaminergic neurons in the murine DRN under control conditions and in a PD model, following striatal injection of the catecholamine toxin, 6-hydroxydopamine (6-OHDA). Electrical and morphological properties of both neuronal populations were altered by 6-OHDA. In serotonergic neurons, most changes were reversed when 6-OHDA was injected in combination with desipramine, a noradrenaline reuptake inhibitor, protecting the noradrenergic terminals. Our results show that the depletion of both noradrenaline and dopamine in the 6-OHDA mouse model causes changes in the DRN neural circuitry.

Introduction

Parkinson's Disease (PD) is a frequent neurodegenerative disorder characterized by the progressive loss of dopaminergic (DA) neurons in the nigrostriatal pathway, leading to bradykinesia, tremor, rigidity, and postural instability [1, 2]. These cardinal motor symptoms are typically addressed by administration of dopaminergic drugs or by deep brain stimulation. PD patients also experience non-motor symptoms including sleep, affective, and cognitive dysfunctions often preceding the motor disabilities [3, 4]. These comorbidities are in large part refractory to current PD treatments and are thought to be caused by neurodegenerative processes occurring in concomitance to the loss of midbrain dopaminergic neurons. However, the pathology underlying non-motor symptoms remains poorly understood.

Post-mortem studies in PD patients provided first insights into the brain areas which might be involved in the etiology of non-motor dysfunctions in PD. Besides the profound degeneration of the substantia nigra pars compacta (SNc), these studies found cell loss and reduced neurotransmitter release in other monoaminergic brain regions, including the dorsal and median raphe nuclei (DRN and MRN, respectively), and the locus coeruleus (LC) [1, 5-8]. The DRN constitutes the main source of serotonin in the brain with serotonergic cells ($DRN^{5\text{-}HT}$) accounting for 30-50% of its neurons [9]. $DRN^{5\text{-}HT}$ neurons have been implicated in numerous neuropsychiatric diseases, rendering them a potential neural substrate for non-motor symptoms in PD. $DRN^{5\text{-}HT}$ neurons are also of central interest in PD research because of their bidirectional, monosynaptic connection with the striatum [10, 11]. In fact, several studies have shown that serotonergic markers and transmitter levels are altered in Parkinson patients as well as in non-human primate and rodent models of PD [12-19]. Notably, alterations in the serotonergic system have also been related to non-motor comorbidities in PD [20, 21]. Yet, functional investigations of $DRN^{5\text{-}HT}$ in rodent models of PD have led to conflicting results showing both increased and decreased activity in $DRN^{5\text{-}HT}$ neurons themselves as well as in their downstream targets [22-24]. Besides the serotonergic neurons, the DRN comprises other neuronal populations, including a small group (~1000 neurons in rats) of DA neurons (DRN^{DA})[25]. DRN^{DA} neurons have been linked to the regulation of pain, motivational processes, incentive memory, wakefulness and sleep-wake transitions [26-30], but their ultimate behavioral significance is yet to be elucidated [31-35]. DRN^{DA} neurons are directly innervated by dopaminergic neurons in the midbrain and have been found to show Lewy bodies in PD patients [6, 30, 36]. Yet, the physiology and pathophysiology of DRN^{DA} neurons in PD remains elusive. The sparsity of research on DRN^{DA} neurons is likely due to the technical challenges associated with targeting this population among the diverse cell types in the DRN and adjacent structures (e.g., retrorubral field, periaqueductal grey and LC), which often co-express signature genes, hampering their molecular identification and region-specific manipulations with cre driver lines [9, 36-39].

Recently, this issue has been addressed by Pinto and colleagues who showed that DRN^{DA} neurons are most faithfully labelled in transgenic mice in which the expression of cre is linked to the DA transporter (DAT-cre) [36]. Previously, the membrane properties of DRN^{DA} neurons have only been addressed in mice in which DRN^{DA} neurons were identified based on the expression of the transcription factor Pitx3 or the enzyme tyrosine hydroxylase (TH) [37]. In Pitx3-GFP mice, about 70% of GFP-positive neurons are TH-positive (TH+) as shown by immunohistochemistry. Moreover, 40% of TH+ neurons in the DRN are not labelled in these mice, suggesting that this line targets a subpopulation of DRN^{DA} neurons [37]. The widely used TH-cre reporter line has been found to show ectopic expression of cre in non-dopaminergic neurons, probably caused by a transient developmental expression of TH [40, 41]. In addition, the TH-cre line also labels noradrenergic neurons in the neighboring LC [40], which produces most of the noradrenaline (NA) in the brain and is involved in mood control, cognition, and sleep regulation [42]. The large overlap of functions ascribed to the LC and DRN is thought to result from the complex reciprocal synaptic connections between these two brain areas: notably, the LC provides noradrenergic input to the DRN [43, 44] while receiving input from $DRN^{5\text{-}HT}$ neurons [45-47].

Here, we used ex vivo whole-cell patch clamp recordings and morphological reconstructions to characterize the electrophysiological and morphological properties of DRN^{DA} and $DRN^{5\text{-}HT}$ neurons in wild type and DAT-tdTomato mice. Moreover, we studied the impact of catecholamine depletion on DRN^{DA} and $DRN^{5\text{-}HT}$ populations in the 6-OHDA toxin model of PD.

83 # Results

84 ## DRN^{DA} and $DRN^{5\text{-}HT}$ neurons are electrophysiologically distinct cell-types

85 To investigate the electrophysiological and morphological profile of DRN^{DA} neurons and to compare it to
86 $DRN^{5\text{-}HT}$ neurons, we performed whole-cell patch clamp recordings in coronal slices of adult wild type and
87 DAT-cre mice crossed with tdTomato reporter mice (Figure 1A). All neurons were filled with neurobiotin
88 and Alexa488 while recording. Alexa488 allowed us to take snapshots of recorded neurons at different time
89 points, thus facilitating the topographical registration of recorded neurons to the post-hoc stained slices
90 (Suppl. Figure 1). Using this approach, we obtained complete sets of electrophysiological and morphological
91 data from 75 neurons in the DRN. Cells were identified as $DRN^{5\text{-}HT}$ or DRN^{DA} neurons based on tryptophan
92 hydroxylase (TPH) or TH immunoreactivity, respectively (Figure 1A-D). In line with Fu et al. (2010)[38], none
93 of the recorded neurons was positive for both TPH and TH (n = 0/412). During the recordings, we used a
94 series of depolarizing and hyperpolarizing current steps and ramps that allowed us to characterize active
95 and passive membrane properties in detail (Figure 1E – G). Based on the electrophysiological data, we first
96 tested possible differences between TH+ neurons recorded in wild-type mice and tdTomato-positive
97 (tdTomato+) neurons recorded in DAT-tdTomato mice. We found no differences between these two groups
98 (n = 13 TH+ vs n = 30 tdTomato+ neurons, Suppl. Figure 2A) and neither within the subset of tdTomato+
99 neurons when comparing TH+ to TH-negative (TH-) neurons (n = 23 TH+ vs n = 6 TH- neurons, Suppl. Figure
100 2A–E). Since this small number of TH- neurons were positive for DAT and their electrophysiology
101 indistinguishable from TH+ DRN^{DA} neurons, the data was pooled. Please note that staining of recorded
102 neurons, i.e. immunohistochemistry on slices strained by hour-long patch-clamp recordings, is more
103 challenging as neurons can be lost after patching (no staining data) or the staining might be ambiguous.
104 Out of 114 tdTomato+ neurons only one cell displayed a different electrophysiological profile than all other
105 DRN^{DA} neurons, suggesting a false-positive rate of 0.8%. That neuron was TH-,displayed profoundly distinct
106 intrinsic properties, and was therefore excluded (Suppl. Figure 2F, G). Taken together, the
107 electrophysiological results support the use of the DAT-tdTomato mouse line when studying DRN^{DA} neurons
108 and data from both mouse lines were pooled. Recordings of DRN^{DA} neurons revealed distinctive
109 electrophysiological properties such as a slowly ramping membrane potential during constant current
110 injections giving rise to delayed spiking and postinhibitory hypoexcitability (Figure 1E). Moreover, most
111 DRN^{DA} neurons displayed rebound oscillations and sag currents (Figure 1E, F).
112 When comparing the electrophysiological properties of DRN^{DA} to $DRN^{5\text{-}HT}$ neurons, we observed numerous
113 differences between these two cell types, but here we focus on the five most significant ones. While $DRN^{5\text{-}HT}$
114 neurons spike with short delays in response to current steps and maintain a relatively constant action
115 potential (AP) amplitude, DRN^{DA} neurons display a longer delay to the first spike and the amplitude of
116 subsequent APs drops (Figure 1F-I). Additionally, the APs of $DRN^{5\text{-}HT}$ neurons rise faster, while their
117 afterhyperpolarization (AHP) is longer compared to DRN^{DA} neurons (Figure 1H, I). Lastly, the capacitance of
118 $DRN^{5\text{-}HT}$ neurons is significantly larger than in DRN^{DA} neurons (Figure 1I).
119 Next, we tested if DRN^{DA} neurons can be distinguished from $DRN^{5\text{-}HT}$ neurons based on these five
120 electrophysiological parameters. To this end, we standardized the data and ran a principal component
121 analysis (PCA) including all $DRN^{5\text{-}HT}$ neurons (i. e. all TPH-positive, TPH+), all TH+ neurons recorded in wild-
122 type mice and all tdTomato+ cells recorded in DAT-tdTomato mice (except for one outlier shown in Suppl.
123 Figure 2F, G). Plotting the first two principal components (PC) showed two separate clusters (Figure 1J,

124 insert). Unsupervised hierarchical cluster analysis based on PC1 and PC2 revealed the same two major
125 clusters and potential subclusters (Figure 1J). Mapping the molecular identity of the cells onto the
126 dendrogram revealed the separation of $DRN^{5\text{-}HT}$ and DRN^{DA} neurons, while there was no branching
127 according to mouse line (wild type vs. DAT-tdTomato), further corroborating the validity of DAT-tdTomato
128 mice as a marker for DRN^{DA} neurons. Overall, these data suggest that electrophysiological parameters
129 themselves are sufficient to distinguish between $DRN^{5\text{-}HT}$ and DRN^{DA} neurons.
130 In addition to DRN^{DA} and $DRN^{5\text{-}HT}$ the DRN contains an unknown number of cell types and 47 out of 120
131 recorded neurons were neither TH+, nor TPH+ and did not express tdTomato. To test whether DRN^{DA} can
132 also be distinguished from those populations based on their electrophysiological profile, we ran a PCA on
133 20 standardized parameters and used the first three PCAs for unsupervised hierarchical clustering (Suppl.
134 Figure 3). Our analysis suggests that there might be four major electrophysiological cell types in the DRN.
135 In contrast to DRN^{DA} and $DRN^{5\text{-}HT}$ neurons, a large proportion of the remaining cells showed rebound spiking
136 and biphasic AHPs, resembling the profiles of local interneurons in other brain areas (Suppl. Figure 3D, E).
137 Interestingly, the clustering also indicated that three TH- and tdTomato-negative (tdTomato-) neurons
138 belonged to the DRN^{DA} neurons and further analysis showed that they were indistinguishable from
139 molecularly identified DRN^{DA} neurons (Suppl. Figure 3C, F). These findings indicate that clustering can be
140 used to identify neurons that otherwise would have been excluded due to a lack of post-hoc staining data
141 or genetic driver lines.
142 Overall, our data show that DRN^{DA} neurons constitute an electrophysiologically distinct class of neurons in
143 the DRN expressing several hallmark properties, which are sufficient to identify them within the local DRN
144 circuitry.
145
146 **DRN^{DA} and $DRN^{5\text{-}HT}$ neurons have different morphological properties**
147 Next, we characterized the morphological profile of $DRN^{5\text{-}HT}$ and DRN^{DA} neurons. We focused on the analysis
148 of somatic and dendritic properties since a complete reconstruction of the axonal arborization could not
149 be retrieved from the slices. The analysis of the somatic properties showed that $DRN^{5\text{-}HT}$ neurons had larger
150 cell bodies than DRN^{DA} neurons (Figure 2A, B), as measured in their area, perimeter, length, and width
151 (Figure 2B). Cell bodies also differed in shape, with DRN^{DA} neurons having more circular somata than $DRN^{5\text{-}}$
152 ^{HT} neurons, as indicated by the circularity index (Figure 2B). Analyzing the dendritic properties, we found
153 that $DRN^{5\text{-}HT}$ neurons had four to five primary dendrites, compared to only two to three in DRN^{DA} neurons
154 (Figure 2A, C). Moreover, dendrites of DRN^{DA} neurons were frequently bipolar with the main primary
155 dendrites starting from opposite extremes of the soma. Both populations had relatively few bifurcations
156 (Figure 2C), but the $DRN^{5\text{-}HT}$ neurons had significantly more terminations (Figure 2C). The overall dendritic
157 length did not differ between the $DRN^{5\text{-}HT}$ and DRN^{DA} neurons: both populations had a mix of short and long
158 dendrites (Figure 2C). These data suggest that $DRN^{5\text{-}HT}$ neurons have denser dendritic arborization than
159 DRN^{DA} neurons, mostly due to larger numbers of primary dendrites.
160 Altogether, our results show that $DRN^{5\text{-}HT}$ and DRN^{DA} neurons have distinct morphological properties. $DRN^{5\text{-}}$
161 ^{HT} neurons are mostly multipolar neurons, with a big and complex soma and multiple primary dendrites,
162 while DRN^{DA} neurons have smaller and more circular cell bodies with bipolar dendrites.
163
164 **DA and NA depletion distinctly affect the membrane properties of $DRN^{5\text{-}HT}$ neurons**

165 To elucidate how $DRN^{5\text{-}HT}$ and DRN^{DA} neurons might be affected in PD, we characterized these populations
166 in a mouse model of PD based on bilateral injection of the neurotoxin 6-OHDA in the dorsal striatum. This
167 approach leads to a partial lesion of catecholamine neurons, reproducing an early stage of parkinsonism in
168 which particularly non-motor symptoms such as depression- and anxiety-like behavior are manifested [48,
169 49]. In line with previous studies, we observed a 60-70% reduction of TH levels in the striatum (Suppl. Figure
170 4, [50]). Only mice meeting this criterion were included in the study. Measurement performed by ELISA
171 showed that the 6-OHDA injection did not alter the levels of 5-HT in the striatum (Suppl. Figure 4D), and
172 immunostaining showed that the striatal 6-OHDA injection did not cause degeneration of $DRN^{5\text{-}HT}$ or DRN^{DA}
173 neurons (Suppl. Figure 5).
174 Striatal injection of 6-OHDA has also been found to produce a partial loss of NA neurons in the LC [50] and
175 ELISA analysis showed that this approach induces approximately 60% loss of NA in the striatum (Suppl.
176 Figure 4E). In the present study, we determined the specific impact of NA dysfunction on the physiology of
177 $DRN^{5\text{-}HT}$ and DRN^{DA} neurons by pre-treating a group of mice with desipramine (DMI), a selective inhibitor of
178 NA reuptake, before injecting 6-OHDA (DMI+6-OHDA mice), which partially prevents striatal NA loss (Suppl.
179 Figure 4E). We then assessed the intrinsic properties of $DRN^{5\text{-}HT}$ and DRN^{DA} neurons in Sham-lesion (Sham),
180 6-OHDA- and DMI+6-OHDA-treated mice (Figure 3A). Whole-cell recordings obtained from $DRN^{5\text{-}HT}$ neurons
181 in control mice revealed that 37% of $DRN^{5\text{-}HT}$ neurons were spontaneously active in slices and the
182 proportion of intrinsically active neurons was similar in mice injected with 6-OHDA (Sham: n = 11/30 $DRN^{5\text{-}}$
183 ^{HT} neurons, 6-OHDA: n = 6/17 $DRN^{5\text{-}HT}$ neurons, Figure 3B). However, $DRN^{5\text{-}HT}$ neurons recorded in DMI+6-
184 OHDA mice showed an increased excitability: in this condition, 72% of $DRN^{5\text{-}HT}$ neurons were spontaneously
185 active and $DRN^{5\text{-}HT}$ neurons displayed lower rheobase currents than control mice (Figure 3B, C). Because
186 of the protective effect exerted in these mice by DMI , these findings suggest that the p noradrenergic
187 system contributes to the increased firing of $DRN^{5\text{-}HT}$ neurons.
188 While the rheobase of $DRN^{5\text{-}HT}$ neurons was not affected in 6-OHDA mice, we observed that their firing
189 properties were profoundly altered: $DRN^{5\text{-}HT}$ neurons recorded in 6-OHDA mice displayed smaller APs than
190 Sham mice and shorter AHPs than both Sham and 6-OHDA injected mice pre-treated with DMI (Figure 3D-
191 F). In contrast, the APs and AHPs of Sham and 6-OHDA injected mice pretreated with DMI did not differ.
192 Moreover, $DRN^{5\text{-}HT}$ neurons of 6-OHDA injected mice fired at higher frequencies than 6-OHDA injected mice
193 pretreated with DMI (Figure 3G-I). Finally, the membrane time constant of $DRN^{5\text{-}HT}$ neurons was shorter in
194 6-OHDA injected mice than in Sham mice (Figure 3J). Interestingly, we found no differences in the firing
195 properties of $DRN^{5\text{-}HT}$ neurons recorded in Sham and in 6-OHDA injected mice pre-treated with DMI,
196 suggesting that the noradrenergic lesion critically contributes to the changes in 6-OHDA mice. Taken
197 together, these results indicate that $DRN^{5\text{-}HT}$ neurons are affected in the 6-OHDA mouse model of PD.
198 Specifically, lesions of the dopaminergic system increase the excitability of $DRN^{5\text{-}HT}$ neurons whereas the
199 combined lesion of the noradrenergic and dopaminergic systems changes the firing properties of $DRN^{5\text{-}HT}$
200 neurons.
201
202 **Striatal DA depletion induces hypotrophy of $DRN^{5\text{-}HT}$ neurons**
203 Morphological analysis revealed a reduced soma size of the $DRN^{5\text{-}HT}$ neurons in 6-OHDA mice, which was
204 manifested as decreased area, perimeter, and major axes in comparison to control mice (Figure 4A-C).
205 Moreover, the increase in the circularity of the 6-OHDA group indicated that the shape of the soma of $DRN^{5\text{-}}$
206 ^{HT} neurons was also altered by the lesion (Figure 4C). These modifications were not observed in DMI + 6-

207 OHDA mice, suggesting that preserving the NA system protected the $DRN^{5\text{-}HT}$ neurons (Figure4A-C). Finally,
208 the injection of 6-OHDA without DMI pre-treatment also resulted in a trend toward reduced number of
209 primary dendrites and terminations of $DRN^{5\text{-}HT}$ neurons (Figure 4D). The number of bifurcations and the
210 dendritic length were not affected by the lesion (Figure 4D). Globally, these results suggest that the lesion
211 produced by 6-OHDA induces a hypotrophic phenotype in $DRN^{5\text{-}HT}$ neurons characterized by a shrinkage of
212 the soma and that this alteration is NA-dependent.
213
214 **Striatal DA depletion affects the firing of DRN^{DA} neurons independent of NA loss**
215 Finally, we assessed whether the striatal 6-OHDA lesion affects the physiology of DRN^{DA} neurons. Whole-
216 cell patch-clamp recordings revealed that 58% of DRN^{DA} neurons are spontaneously active in slices of Sham-
217 lesion mice (Figure 5A). In contrast, the proportion of intrinsically active neurons increased to 77% and 78%
218 of DRN^{DA} neurons in 6-OHDA injected mice with and without pre-treatment with DMI, respectively.
219 In stark contrast to $DRN^{5\text{-}HT}$ neurons, the rheobase, the APs and their AHPs, the IF slope and the time
220 constant of DRN^{DA} neurons were not affected in any 6-OHDA mice (Figure 5B-I). In fact, we did not observe
221 any change in the firing properties of DRN^{DA} neurons that was dependent on the protection of the NA
222 system with DMI (Figure 5). DRN^{DA} neurons recorded in 6-OHDA injected mice pre-treated with DMI did
223 however display a reduction in spike latency compared to Sham-lesioned mice (Figure 5G). Together, these
224 results suggest that the electrophysiological properties of DRN^{DA} neurons are affected in the 6-OHDA
225 mouse model of PD and that these changes are primarily due to the lesion of the nigrostriatal dopaminergic
226 pathway.
227 **Striatal DA depletion does not change significantly the morphology of DRN^{DA} neurons**
228 The morphological analysis of DRN^{DA} neurons revealed that the striatal 6-OHDA injection did not
229 significantly affect somatic and dendritic morphology.
230 **Unilateral lesion of LC NA cells induces minor changes in DRN subpopulations**
231 Our results so far suggest that concomitant lesioning of the DA and NA system (6-OHDA model) has a severe
232 impact on $DRN^{5\text{-}HT}$ neurons which cannot be evoked when the NA system is partially protected (DMI + 6-
233 OHDA model). Therefore, we next assessed if selective lesioning of the NA system itself is sufficient to evoke
234 changes in electrical and morphological properties observed in $DRN^{5\text{-}HT}$ neurons recorded in 6-OHDA. To
235 that end we performed unilateral injections of 6-OHDA/saline in the LC (Suppl. Figure 6A), which lead to
236 approximately 50% loss of TH+ neurons in the LC (Suppl. Figure 6B, C). We chose to restrict the injection of
237 6-OHDA to one hemisphere because little is known about this type of lesion while the fundamental role of
238 the NA system in various neural processes is well established [51, 52]. We found that selective lesioning of
239 the LC ('6-OHDA-LC') did not alter the baseline activity levels, firing frequencies and resting membrane
240 potentials of $DRN^{5\text{-}HT}$ and DRN^{DA} neurons (Suppl. Fig. 6D, E, K, L). However, $DRN^{5\text{-}HT}$ neurons recorded in 6-
241 OHDA-LC had a lower input resistance at hyperpolarized membrane potentials, a shorter
242 afterhyperpolarization and a larger capacitance than $DRN^{5\text{-}HT}$ neurons recorded in control mice (Sham-LC,
243 Suppl. Fig. 6E-G). Moreover, DRN^{DA} neurons recorded in 6-OHDA-LC showed a reduction in their sag
244 amplitudes (Suppl. Fig 6M, N). The other electrophysiological parameters were not significantly affected.
245 Morphological analysis revealed that the selective lesion of the noradrenergic system did not alter the size
246 and shape of cell bodies in either DRN subpopulation (Suppl. Figure 6H,I, O,P), however, the dendritic
247 branching of both subpopulations was altered, as shown by the increased length of primary dendrites in

248 DRN$^{5\text{-}HT}$neurons (Suppl. Figure 6J) and the increased number of primary dendrites in DRN^{DA} neurons (Suppl.
249 Figure 6Q).
250
251 ## Discussion
252 In the present study we combine *ex vivo* whole-cell patch clamp recordings with morphological
253 reconstructions and immunohistochemistry, to show that DRN^{DA} neurons have a distinct
254 electrophysiological profile, which is sufficient to distinguish them from DRN$^{5\text{-}HT}$ neurons as well as other
255 neuron classes in the DRN. Utilizing this approach, we also reveal that, in a 6-OHDA mouse model of PD,
256 DRN$^{5\text{-}HT}$ neurons display distinct pathophysiological changes depending on the loss of DA and NA. Notably,
257 degeneration of noradrenergic neurons affects not only the electrical properties of DRN$^{5\text{-}HT}$ neurons but
258 also evokes hypotrophy of their cell bodies. In contrast, the loss of nigrostriatal DA mainly affects the
259 electrophysiological properties of DRN^{DA} neurons while concomitant loss of NA alters their morphology.
260
261 We used an extensive electrophysiological characterization protocol to quantify the differences between
262 the DRN^{DA} and DRN$^{5\text{-}HT}$ populations. The electrophysiological properties agree with previous studies, such
263 as the spontaneous firing pattern seen in DRN^{DA} neurons [37], and the slow AHP of DRN$^{5\text{-}HT}$ neurons [23].
264 Standard electrophysiological parameters were used to create a classification tool, which efficiently
265 identifies DRN$^{5\text{-}HT}$ and DRN^{DA} cells, including DA neurons confirmed by TH staining and / or by fluorescent
266 expression in DAT-tomato mice (Figure 1). Importantly, the DRN^{DA} neurons recorded from wild-type and
267 DAT-tdTomato mice did not differ in their electrical properties, indicating that the transgene does not
268 interfere with the membrane properties of this population.
269
270 We showed that DRN^{DA} neurons share electrophysiological properties with other dopaminergic populations
271 in the midbrain such as postinhibitory hypoexcitability, rebound oscillations, a slowly ramping membrane
272 potential and sag currents [37, 53, 54], yet their electrophysiological profile is distinct from DRN$^{5\text{-}HT}$ neurons
273 as well as other neuronal populations in the DRN. Most of the parameters extracted in our characterization
274 rely on intracellular recordings of the membrane potential. However, some properties such as spontaneous
275 firing and AP kinetics could be useful for *in vivo* characterization, even in extracellular recordings [55-57].
276 In addition to the DRN$^{5\text{-}HT}$ and DRN^{DA} neuronal populations, a large fraction of neurons displayed
277 electrophysiological properties that were distinct from these two groups (Suppl. Figure 3), suggesting that
278 there are other neuronal subtypes in the DRN network, such as previously reported GABAergic,
279 glutamatergic, and peptidergic neurons [9, 10, 58-62].
280
281 In line with previous studies, the majority of DRN$^{5\text{-}HT}$ neurons were large multipolar or fusiform neurons
282 with four to five primary dendrites, very distinct from the DRN^{DA} neurons [63-65]. Very little is known about
283 the morphology of the DRN^{DA} neurons, but previous studies identified small ovoid cells in the DRN which
284 are likely to correspond to the DRN^{DA} cells [37, 66]. Out of 25 reconstructed DRN$^{5\text{-}HT}$ neurons, only one
285 displayed dendritic spines. Previous studies in rats described the presence of dendritic spines in most DRN$^{5\text{-}}$
286 ^{HT} neurons [67]. However, the study was performed in thicker slices and the dendritic spines were scarce
287 in the primary and secondary dendrites, while they became dense in the distal dendrites, thus it is possible
288 that in our study those dendrites were not present [67].
289

290 In the present study we assessed the impact on DRN cells of a striatal bilateral 6-OHDA lesion performed
291 with or without DMI pre-treatment, which has been shown to protect the NA neurons in the LC from the
292 6-OHDA-induced degeneration [50, 68, 69]. We found that both $DRN^{5\text{-}HT}$ and DRN^{DA} populations were
293 affected in a cell-type specific manner by the combined action of 6-OHDA on DA and NA, with $DRN^{5\text{-}HT}$
294 neurons being particularly sensitive to changes in the noradrenergic system. Loss of SNc dopaminergic
295 neurons alone (6-OHDA + DMI) – which are known to target $DRN^{5\text{-}HT}$ and DRN^{DA} neurons directly – increased
296 the excitability and spontaneous activity in $DRN^{5\text{-}HT}$ neurons [10]. This is in line with previous *ex vivo* and *in*
297 *vivo* studies showing that the $DRN^{5\text{-}HT}$ neurons display increased firing rates in rodents pre-treated with DMI
298 and injected with 6-OHDA [23, 70] As hypothesized by Prinz et al. [23], the selective loss of midbrain DA
299 may induce a homeostatic increase in the excitability of $DRN^{5\text{-}HT}$ neurons. Our data contrast with a previous
300 *in vivo* study showing decreased firing activity in $DRN^{5\text{-}HT}$ neurons where injection of 6-OHDA was preceded
301 by treatment with DMI and fluoxetine [24]. This dissimilarity may be related to species-specific (rat vs
302 mouse) and technical (intracerebroventricular vs striatal injections, recordings performed at 10 days vs
303 three weeks after the 6-OHDA injection). Importantly, in the same study identification of $DRN^{5\text{-}HT}$ neurons
304 was not molecularly confirmed and the data may include other spontaneously active DRN neurons. In fact,
305 our recordings show that there are non-serotonergic neurons in the DRN, which are spontaneously active
306 and display a regular, slow firing frequency similar to $DRN^{5\text{-}HT}$ neurons, highlighting the importance of
307 unequivocal identification of DRN cell types.
308
309 The present study shows that combined DA and NA lesioning affects $DRN^{5\text{-}HT}$ neurons more profoundly than
310 selective loss of DA (Figure 3, 4). In mice treated with 6-OHDA only, several electrophysiological and
311 morphological properties were altered (Figure 3, 4). The time constant and AHP of $DRN^{5\text{-}HT}$ neurons were
312 shorter and the neurons responded with higher firing frequencies to current injections than in Sham. This
313 finding suggests that the pronounced AHP and long tau of these neurons may act as a "brake" limiting their
314 maximum firing frequency in control conditions and that this brake is reduced when the NA system is
315 lesioned. Future studies are needed to assess if $DRN^{5\text{-}HT}$ neurons in fact fire at higher rates in vivo in mice
316 treated with 6-OHDA. In contrast, such changes in $DRN^{5\text{-}HT}$ neurons were prevented when the NA system
317 was protected by pre-treatment with DMI. These findings indicate an important role for NA as mediator of
318 changes in the activity and properties of $DRN^{5\text{-}HT}$ neurons. The changes produced by the 6-OHDA lesion on
319 the DRN^{DA} population were less pronounced than and different from those in $DRN^{5\text{-}HT}$ neurons. In terms of
320 electrophysiological properties, the observed changes were primarily in the DA only lesion (6-OHDA + DMI),
321 suggesting that unlike $DRN^{5\text{-}HT}$, DRN^{DA} neurons are affected by the loss of midbrain DA rather than the
322 accompanying changes in NA (Figure 5). Interestingly, unilateral lesions in the LC did not result in significant
323 alterations in DRN neurons to the extent of the larger striatal lesions (Suppl. Figure 6). Although the trends
324 of some of the electrophysiological parameters, such as the amplitude and duration of the AP and the AHP
325 observed in $DRN^{5\text{-}HT}$ neurons, were similar to those induced by the 6-OHDA only lesion shown in Figure 3,
326 the effects were smaller. This could be due to the more limited extent of the LC injections compared to the
327 striatal ones as well as the unilateral LC vs. bilateral striatal lesioning. These two factors may have reduced
328 the impact of NA depletion and should be further investigated in future studies.
329
330 Our results show that DRN neurons are affected by depletion of both DA and NA, thus raising the possibility
331 that non-motor symptoms in PD are a result of the intricate organization of DA and NA neuromodulation

332 as well as the interactions between the different DRN neuronal populations. Moreover, our results highlight
333 the complex interplay in the DRN between NA, DA, and 5-HT, but the precise pathophysiological processes
334 resulting from loss of NA, and specifically the impact on DRN, are yet to be elucidated.
335
336 In conclusion, our study provides a quantitative description and classification scheme for two major
337 neuronal populations in the DRN, $DRN^{5\text{-}HT}$ and DRN^{DA} neurons. We identified novel electrophysiological and
338 morphological changes in these populations in response to DA and NA depletion in the basal ganglia.
339 Considering the involvement of DRN and LC in the development of non-motor comorbidities, this study
340 provides useful insights to understand better how these areas are affected in the parkinsonian condition.
341 Moreover, our data pave the way for future experiments to characterize these subpopulations in terms of
342 receptor expression and synaptic connectivity to shed light on their functional roles particularly with regard
343 to the wide variety of non-motor symptoms observed in PD.

Methods

Experimental model details

All animal procedures were performed in accordance with the national guidelines and approved by the local ethics committee of Stockholm, Stockholms Norra djurförsöksetiska nämnd, under ethical permits to G. F. (N12148/17, 14673-22) and G. S. (N2020/2022). All mice (N=43) were group-housed under a 12 hr light / dark schedule and given ad libitum access to food and water. Wild-type mice ('C57BL/6J', #000664, the Jackson laboratory) and DAT-cre (Stock #006660 the Jackson laboratory) mice crossed with homozygous tdTomato reporter mice ('Ai9', stock #007909, the Jackson laboratory) were used.

6-OHDA model

Three-months old, male and female C57BL/6J or DAT-tdTomato were deeply anesthetized with Isoflurane and mounted on a stereotaxic frame (Stoelting Europe, Dublin, Ireland). To achieve a partial striatal lesion, each mouse received a bilateral injection of 1.25 µl of 6-hydroxydopamine hydrochloride (6-OHDA, Sigma-Aldrich, 4µg/µl) or vehicle (0.9 % NaCl + Ascorbic Acid 0.02%) in the dorsolateral striatum, according to the following coordinates: anteroposterior +0.6 mm, mediolateral ± 2.2, dorsoventral -3.2 from Bregma, as previously described [48, 71]. One group of mice (referred to as DMI + 6-OHDA) was pre-treated with one injection of desipramine hydrochloride (DMI, Sigma-Aldrich, 25mg/kg i.p.) 30 minutes before the 6-OHDA infusion in order to protect the noradrenergic system [50].

For the LC lesion, mice received a unilateral injection of 1 µl of 6-OHDA (Sigma-Aldrich, 4µg/µl) or vehicle (0.9 % NaCl + Ascorbic Acid 0.02%) according to the following coordinates: anteroposterior –5.4 mm, mediolateral –0.9, dorsoventral -3.8 from Bregma.

Slice preparation and electrophysiology

Three weeks after the 6-OHDA/vehicle injection, mice were deeply anaesthetized with isoflurane and decapitated. The brain was quickly removed and immersed in ice-cold cutting solution containing 205 mM sucrose, 10 mM glucose, 25 mM NaHCO3, 2.5 mM KCl, 1.25 mM NaH2PO4, 0.5 mM CaCl2 and 7.5 mM MgCl2. In all experiments, the brain was divided into two parts: the striatum was dissected from the anterior section for Western Blot and the posterior part was used to prepare coronal brain slices (250 µm) with a Leica VT 1000S vibratome. Slices were incubated for 30-60 min at 34°C in a submerged chamber filled with artificial cerebrospinal fluid (ACSF) saturated with 95% oxygen and 5% carbon dioxide. ACSF was composed of 125 mM NaCl, 25 mM glucose, 25 mM NaHCO3, 2.5 mM KCl, 2 mM CaCl2, 1.25 mM NaH2PO4, and 1 mM MgCl2. Subsequently, slices were kept for at least 60 min at room temperature before recording. Whole-cell patch clamp recordings were obtained in oxygenated ACSF at 35°C. Neurons were visualized using infrared differential interference contrast (IR-DIC) microscopy (Zeiss FS Axioskop, Oberkochen, Germany). DAT-tdTomato positive cells were identified by switching to epifluorescence using a mercury lamp (X-cite, 120Q, Lumen Dynamics). Up to three cells were patched simultaneously. Borosilicate glass pipettes (Hilgenberg) of 6 - 8 MOhm resistance were pulled with a Flaming / Brown micropipette puller P-1000 (Sutter Instruments). The intracellular solution contained 130 mM K-gluconate, 5 mM KCl, 10 mM HEPES, 4 mM Mg-ATP, 0.3 mM GTP, 10 mM Na2-phosphocreatine (pH 7.25, osmolarity 285 mOsm), 0.2% neurobiotin (Vector laboratories, CA) and Alexa-488 (75 µM) was added to the intracellular solution

385 (Invitrogen). Recordings were made in current-clamp mode and the intrinsic properties of the neurons
386 were determined by a series of hyperpolarizing and depolarizing current steps and ramps, enabling the
387 extraction of sub- and suprathreshold properties. Recordings were amplified using MultiClamp 700B
388 amplifiers (Molecular Devices, CA, USA), filtered at 2kHz, digitized at 10-20kHz using ITC-18 (HEKA
389 Elektronik, Instrutech, NY, USA), and acquired using custom-made routines running on IgorPro
390 (Wavemetrics, OR, USA). Throughout all recordings pipette capacitance and access resistance were
391 compensated for and data were discarded when access resistance increased beyond 30 MOhm. Liquid
392 junction potential was not corrected for.
393
394 Quantification of electrophysiological parameters
395 Immediately after obtaining a whole-cell patch in DRN neurons, we first obtained a 10s voltage recording
396 of the neural activity without injecting any current. This recording was used to calculate the average resting
397 membrane potential in silent neurons and the firing frequency of spontaneously active neurons.
398 Subsequently, neurons were held at –60mV while an extensive series of de- and hyperpolarizing current
399 steps was applied. The amplitude of all current steps was scaled according to a test pulse that was set to
400 evoke one to two AP. The resulting voltage recordings were used to extract and calculate the following
401 parameters: The rheobase was defined as the minimum current required to evoke AP firing. AP parameters
402 were extracted from recordings where $DRN^{5\text{-}HT}$ neurons fired at 1 ± 0.3 Hz and DRN^{DA} neurons at 2 ± 0.3 Hz
403 (i.e. close to their average spontaneous firing frequency) and values from individual APs were averaged. AP
404 onset was extracted by quantifying where the rising slope of the AP (its first derivative) reached 5V/s and
405 the end of the AP was defined as the time where the AP had repolarized to the same membrane voltage as
406 found at the onset. The AP duration was calculated as the time between the onset and the offset. The
407 amplitude of the AP was defined as the voltage difference between the onset and its peak. The amplitude
408 of the AHP was defined as the voltage difference between the end of the AP and the subsequent local
409 minimum. The end of the AHP was found by using a sliding window of 50ms to assess when the slope of
410 the decaying AHP had first decreased to 0.005V/s or less. The AP drop rate was measured by injecting a
411 current ramp into the neurons that evoked multiple APs. The amplitude of these APs was extracted as
412 described above. The amplitude was plotted versus the injected current and a linear fit was applied whose
413 slope constitutes the AP drop rate. The delay to the first spike constitutes the time between the onset of
414 the current injection and the onset of the first AP in recordings. The input resistance was based on the
415 slope of a linear fit across all current–voltage steps that resulted in a steady state voltage between –90 and
416 –50mV (R = U / I). The steady state voltage was based on the average voltage found during a time window
417 starting 0.5s after the beginning of a 1s long current step and lasting until the end of the current step. The
418 amplitude of sag currents was defined as the average voltage difference between the steady state voltage
419 and the peak voltage evoked by current steps that hyperpolarized the neurons to –90 ± 5mV. The peak
420 voltage constituted the minimum voltage observed during the first 0.5s of the step. The time constant tau
421 was extracted following injection of a 5ms long hyperpolarizing current step. We applied an exponential fit
422 to the resulting voltage recording that started 1ms after the negative voltage peak had been reached and
423 ended when the membrane potential had returned to the average baseline voltage preceding the step. Tau
424 corresponds to K2 given the exponential fit is defined as y = K0 + K1*exp(-K2*x). Based on tau and the
425 steady-state input resistance, we calculated the capacitance C according to C = tau / resistance. The IF slope
426 was extracted from the linear fit applied to a current-frequency plot.

427

428 Immunofluorescence

429 Following the recordings, slices were fixated overnight at 4°C in a 4% paraformaldehyde solution. Slices
430 were then washed with PBS 1X. For the immunofluorescence, slices were treated with PBS 1X + Triton 0.3%
431 and then incubated with a blocking solution of Normal Serum 10% and Bovine Serum Albumin 1% for 1h at
432 room temperature. Afterward, slices were incubated overnight at 4°C with the following primary
433 antibodies: rabbit anti-TH (Millipore, 1:1000), mouse anti-TPH (Sigma Aldrich, 1:600) and Streptavidin
434 (Jackson Immunoresearch, 1:500). The following day, primary antibodies were washed out and slices were
435 incubated with the appropriate fluorochrome-conjugated secondary antibodies.
436 For the immunostainings in the striatum, SNc, LC and cell counting in DRN, mice were deeply anesthetized
437 and transcardially perfused with PFA 4%. The brains were extracted and post-fixed in PFA 4% for 24 hours.
438 40 µm coronal slices were prepared with a vibratome (Leica VT1000 S) and processed as described above.
439

440 Confocal Microscopy Analysis

441 The slices were imaged using Confocal (ZEISS LSM 800) at 10X and 40X and z-stacks were retrieved. For cell
442 identification, colocalization between neurobiotin and TH or TPH was evaluated.
443

444 Morphological analysis

445 For morphological analysis of dendrites, the confocal z-stacks were used in a semi-manual reconstruction
446 using neuTube [72] and custom code, as previously described [73]. Soma morphology was analyzed by
447 tracing manually the cell body profile, excluding dendritic trunks, in order to measure area (μm^2),
448 perimeter, major and minor axis length (µm) and circularity values. Circularity, calculated as the ratio
449 between the squared perimeter and the area (i.e. $perimeter^2/4\pi$ area), can be a value between 0 and 1 (1
450 for circular shapes and values < 1 for more complex shapes).
451 The morphological analysis was performed on the neurobiotin stacks.
452

453 Western Blot

454 The striata were sonicated in 1% sodium dodecyl sulfate and boiled for 10 min. Equal amounts of protein
455 (25 µg) for each sample were loaded onto 10% polyacrylamide gels and separated by electrophoresis and
456 transferred overnight to nitrocellulose membranes (Thermo Fisher, Stockholm, Sweden). The membranes
457 were immunoblotted with primary antibodies against actin (1:30,000, Sigma Aldrich, Stockholm, Sweden)
458 and TH (1:2000, Millipore, Darmstadt, Germany). Detection was based on fluorescent secondary antibody
459 binding (IR Dye 800CW and 680RD, Li-Cor, Lincoln, NE, USA) and quantified using a Li-Cor Odyssey infrared
460 fluorescent detection system (Li-Cor, Lincoln, NE, USA). The TH protein levels were normalized for the
461 corresponding actin detected in the sample and then expressed as a percentage of the control (Sham-
462 lesion).
463

464 Enzyme-linked immunosorbent assay

465 NA and 5-HT levels in the striatum were determined by Enzyme-linked immunosorbent assay (ELISA). Three
466 weeks after the 6-OHDA injection, mice were killed by decapitation and the striatum was dissected out
467 freehand on an ice-cold surface and weighted. The tissue was sonicated in a buffer with HCl 0.01M, EDTA
468 1mM and sodium metabisulfite 4 mM (25 µl/mg of tissue). The brain homogenates were centrifuged at 4

469 °C, 13000 rpm for 20 minutes and the supernatants were collected. The samples were assessed in analytic
470 duplicate using Noradrenaline and Serotonin Research ELISA kits (LDN, Germany), according to the
471 manufacturer's instructions. The absorbance at 450 nm was measured using a microplate reader. Tissue
472 concentrations of NA and 5-HT were determined using a standard curve.
473
474
475 Statistical Analysis
476 Statistical analysis was performed using GraphPad Prism 9.2.0. Data were first tested for normality by
477 Kolmogorov-Smirnov test. Two-groups analysis was performed by unpaired t-test for normally distributed
478 data and the Mann-Whitney U test for non-normally distributed data. Three-groups analysis was performed
479 by one-way ANOVA for normally distributed data or Kruskal-Wallis test for non-normally distributed data.
480 Data are reported as average ± SEM. N indicates the number of mice, while n indicates the number of cells.
481 Significance was set at $p<0.05$.
482
483
484
485

Acknowledgments

We thank Elin Dahlberg for technical assistance and Kristoffer Tenebro Berglund for taking care of the mice. We also thank the members of the Silberberg and Fisone labs and the AND-PD consortium members for comments and discussions.

Funding

This work was supported by a Wallenberg Fellowship from the Knut & Alice Wallenberg Foundation (KAW 2017.0273), the Swedish Brain Foundation (Hjärnfonden, FO2021-0333), and the Swedish Medical Research Council (VR-M, 2019-0 1254) to GS, and a Swedish Research Council International Postdoc Grant (2020-06365) to YJ. RT, RA, GF, and GS are supported by an EU grant (H2020 848002 AND-PD).

Author contributions

Conceptualization: LB, YJ, RT, RM, GF, GS.
Investigation: YJ (electrophysiology, clustering analysis), LB (6-OHDA lesions, morphological analysis, cell counting, western blot, ELISA).
Visualization: YJ (electrophysiological and clustering results), LB (6-OHDA model, morphological reconstructions).
Supervision: GS and GF.
Writing—original draft: YJ and LB.
Writing—review & editing: LB, YJ, GF, GS.

Competing Interests

The authors declare that they have no competing interests.

Data availability

All raw data is available upon reasonable request.

512 # Figure Legends

513

514 **Figure 1. DRN^{DA} and $DRN^{5\text{-}HT}$ are electrophysiologically distinct cell-types. (A)** Scheme of the location of the DRN (pink)
515 in a coronal section (top) and at higher magnification together with two patch pipettes (center). Bottom: a
516 representative slice stained post recording for TPH, TH and neurobiotin revealing serotonergic neurons (arrows). The
517 ventricle is indicated with a dashed line. **(B)** Top: differential interference contrast (DIC) microscopy image (left) of
518 neurons that were filled with Alexa488 (right) and neurobiotin. Center, bottom: staining of the same neurons revealing
519 a TPH+ ($DRN^{5\text{-}HT}$) neuron and a TPH- and TH- cell. **(C)** Top: DIC image of recorded neurons that were filled with Alexa488
520 and neurobiotin. Center, bottom: staining of the same neurons revealing tdTomato- and TH+ (DRN^{DA}) neurons. **(D)**
521 Representative fluorescent (top), DIC (center) image and overlay (bottom) of a tdTomato+ neuron in a DAT-tdTomato
522 mouse. **(E)** Representative recordings depicting postinhibitory hypoexcitability, slowly ramping currents and rebound
523 oscillations in DRN^{DA} neurons. **(F)** Representative voltage responses to current injections in a TPH+ ($DRN^{5\text{-}HT}$) and TH+
524 (DRN^{DA}) neuron. **(G)** Ramping current injections reveal action potential (AP) amplitude accommodation. Gray circles
525 indicate the onset and peak of APs. **(H)** Amplitude and duration of the AP and AP afterhyperpolarization (AHP) in a
526 $DRN^{5\text{-}HT}$ and DRN^{DA} neurons. Gray circles indicate onset, peak, and end of the AP and AHP. **(I)** Quantification of
527 electrophysiological properties distinguishing $DRN^{5\text{-}HT}$ from DRN^{DA} neurons (AP drop rate: n = 32 $DRN^{5\text{-}HT}$, n = 43 DRN^{DA},
528 Capacitance: n = 32 $DRN^{5\text{-}HT}$, n = 43 DRN^{DA}, AP delay: n = 30 $DRN^{5\text{-}HT}$, n = 43 DRN^{DA}, AHP duration: n = 28 $DRN^{5\text{-}HT}$, n =
529 32 DRN^{DA}, N = 9; Wilcoxon Rank Sum Test). **(J)** Principal component analysis (PCA) of five electrophysiological
530 parameters (insert) and hierarchical cluster analysis based on PCA1 and PCA2 (Ward's method, Euclidean distance).
531 Intrinsic properties were sufficient to separate TPH+ cells (blue dash) from TH+ (red dash) cells. Bottom dashes
532 indicate wild type (black) and DAT-tdTomato (gray) mice. Data are shown as mean ± SEM, ***$p < 0.001$. Scale bars: A,
533 100 µm; B-D, 10 µm.

534

535 **Figure 2. DRN^{DA} and $DRN^{5\text{-}HT}$ have distinct morphological profiles. (A)** Top: representative digital reconstruction of a
536 $DRN^{5\text{-}HT}$. Bottom: representative digital reconstruction of a DRN^{DA}. **(B-F)** Morphological parameters describing the
537 soma size and shape of $DRN^{5\text{-}HT}$ and DRN^{DA} neurons ($DRN^{5\text{-}HT}$: n = 20, N = 3; DRN^{DA}: n = 27, N = 3; unpaired t-test or
538 Mann-Whitney U test). **(G-J)** Morphological parameters describing the dendritic tree of $DRN^{5\text{-}HT}$ and DRN^{DA} neurons
539 ($DRN^{5\text{-}HT}$: n = 8, N = 3; DRN^{DA}: n = 7, N = 3; Mann-Whitney U test). Data are shown as mean ± SEM, ***$p < 0.001$. Scale
540 bar: 10 µm.

541

542 **Figure 3. Lesions targeting primarily nigrostriatal dopamine increase the excitability of $DRN^{5\text{-}HT}$ neurons whereas loss**
543 **of NA affects their action potentials. (A)** Overview of workflow for analyzing the electrophysiological and
544 morphological properties of DRN neurons in Sham and 6-OHDA lesioned mice. **(B)** Top: pie charts showing the number
545 of spontaneously active (dark) and silent (pale) $DRN^{5\text{-}HT}$ neurons in three conditions: Sham (left), 6-OHDA-injected
546 mice (center) and 6-OHDA-injected mice pre-treated with desipramine (DMI + 6-OHDA, right). Bottom: representative
547 recordings of spontaneously active $DRN^{5\text{-}HT}$ neurons (I = 0 pA). **(C)** Quantification of the rheobase (left, Sham: n = 30,
548 6-OHDA: n = 17, DMI + 6-OHDA: n = 25), the firing frequency of spontaneously active cells (center, Sham: n = 11, 6-
549 OHDA: n = 6, DMI + 6-OHDA: n = 18), and the resting membrane potential of silent $DRN^{5\text{-}HT}$ neurons (right, Sham: n =
550 19, 6-OHDA: n = 11, DMI + 6-OHDA: n = 7). **(D)** Representative action potentials of $DRN^{5\text{-}HT}$ at low (left) and high (right)
551 temporal resolution. Gray circles indicate onset, offset, and peak of the APs as well as the end of the
552 afterhyperpolarization (AHP). **(E)** Quantification of the amplitude (left) and duration (right) of the APs of $DRN^{5\text{-}HT}$
553 neurons (Sham: n = 29, 6-OHDA: n = 16, DMI + 6-OHDA: n = 21). **(F)** Same as in (D) for the AHP. **(G)** Representative
554 responses of $DRN^{5\text{-}HT}$ neurons to current steps (I = +75 pA). **(H)** Quantification of firing frequency / injected current.
555 **(I)** Quantification of the delay to the first AP when injected with current eliciting 1Hz firing (Sham: n = 29, 6-OHDA: n
556 = 16, DMI + 6-OHDA: n = 21). **(J)** Quantification of the membrane time constant (tau) of $DRN^{5\text{-}HT}$ neurons (Sham: n =

557 32, 6-OHDA: n = 16, DMI + 6-OHDA: n = 21). Sham: N = 6 - 7; 6-OHDA: N = 7; DMI + 6-OHDA: N = 4; unpaired t-test or
558 Mann-Whitney U test. Data are shown as mean ± SEM, * $p < 0.05$, ** $p < 0.01$.

559

560 **Figure 4. Striatal injection of 6-OHDA induced a hypotrophic phenotype in the $DRN^{5\text{-}HT}$, which is prevented by pre-**
561 **treatment with DMI. (A)** Representative digital reconstructions of a $DRN^{5\text{-}HT}$ neuron in three different conditions: Sham
562 (left), 6-OHDA-injected mice (center) and 6-OHDA-injected mice pre-treated with desipramine (right). **(B)**
563 Representative confocal pictures of soma from $DRN^{5\text{-}HT}$ neurons in Sham (top), 6-OHDA-injected mice (center), and 6-
564 OHDA-injected mice pre-treated with desipramine (bottom). **(C-G)** Morphological descriptors of the soma size and
565 shape in $DRN^{5\text{-}HT}$ neurons (Sham: n = 20, N = 4; 6-OHDA: n = 19, N = 4; DMI + 6-OHDA: n = 17, N = 3; one-way ANOVA).
566 **(H-K)** Morphological descriptors of the dendritic tree in $DRN^{5\text{-}HT}$ neurons (Sham: n = 8, N = 3, 6-OHDA: n = 6, N = 3:
567 DMI + 6-OHDA: n = 6, N = 2). Data are shown as mean ± SEM, ***$p<0.001$, **$p<0.01$, *$p<0.05$. Scale bar: 10 µm.
568

569 **Figure 5. Lesions targeting primarily SN dopamine depolarize DRN^{DA} neurons whereas concomitant loss of NA does**
570 **not affect their action potentials. (A)** Top: Pie charts showing the proportion of spontaneously active (dark) and silent
571 (pale) DRN^{DA} neurons in three conditions: Sham (left), 6OHDA-injected mice (center) and 6-OHDA-injected mice pre-
572 treated desipramine (DMI, right). Bottom: Representative recordings of spontaneously active DRN^{DA} (I = 0pA). **(B)**
573 Quantification of the rheobase (left, Sham: n = 43, 6-OHDA: n = 31, DMI + 6-OHDA: n = 40), the firing frequency of
574 spontaneously active (center, Sham: n = 25, 6-OHDA: n = 23, DMI + 6-OHDA: n = 31), and the resting membrane
575 potential of silent DRN^{DA} neurons (right, Sham: n = 18, 6-OHDA: n = 7, DMI + 6-OHDA: n = 9). **(C)** Representative action
576 potentials of DRN^{DA} at low (left) and high (right) temporal resolution. Gray circles indicate onset, offset, and peak of
577 APs and the end of the afterhyperpolarization (AHP). **(D)** Quantification of the amplitude (left) and duration (right) of
578 the APs of DRN^{DA} neurons (Sham: n = 34, 6-OHDA: n = 23, DMI + 6-OHDA: n = 35). **(E)** Same as in (D) for the AHP. **(F)**
579 Representative responses of DRN^{DA} neurons to current steps (I = 75pA). Gray circles indicate the delay to the first AP.
580 **(G-I)** Quantification of firing frequency / injected current (G, Sham: n = 31, 6-OHDA: n = 23, DMI + 6-OHDA: n = 27),
581 the delay to the first AP when injected with current eliciting 2 Hz firing (H, Sham: n = 34, 6-OHDA: n = 23, DMI + 6-
582 OHDA: n = 35), and the membrane time constant (I, Sham: n = 43, 6-OHDA: n = 29, DMI + 6-OHDA: n = 40) of DRN^{DA}
583 neurons recorded (Sham: N = 8; 6-OHDA: N = 6; DMI + 6-OHDA: N = 6; unpaired t-test or Mann-Whitney U test). Data
584 are shown as mean ± SEM, * $p < 0.05$.

585 **Figure 6. Striatal injection of 6-OHDA did not alter morphology of DRN^{DA}. (A)** Representative digital reconstructions of
586 a DRN^{DA} neuron in three different conditions: Sham (left), 6-OHDA-injected mice (center) and 6-OHDA-injected mice
587 pre-treated with desipramine (right). **(B)** Representative confocal pictures of soma from DRN^{DA} neurons in Sham (top),
588 6-OHDA-injected mice (center), and 6-OHDA-injected mice pre-treated with DMI (bottom). **(C-G)** Morphological
589 descriptors of the soma size and shape in DRN^{DA} neurons (Sham: n = 27, N = 7, 6-OHDA: n = 16, N = 4; DMI + 6-OHDA:
590 n = 31, N = 5). **(H-K)** Morphological descriptors of the dendritic tree in DRN^{DA} neurons. (Sham: n = 7, N = 3; 6-OHDA: n
591 = 11, N = 4; DMI + 6-OHDA: n = 7, N = 3). Data are shown as mean ± SEM. Scale bar: 10 µm.
592
593
594

References

1. Braak, H., et al., *Staging of brain pathology related to sporadic Parkinson's disease.* Neurobiol Aging, 2003. **24**(2): p. 197-211.
2. Jankovic, J., *Parkinson's disease: clinical features and diagnosis.* J Neurol Neurosurg Psychiatry, 2008. **79**(4): p. 368-76.
3. Swick, T.J., *Parkinson's disease and sleep/wake disturbances.* Parkinsons Dis, 2012. **2012**: p. 205471.
4. Chaudhuri, K.R. and A.H. Schapira, *Non-motor symptoms of Parkinson's disease: dopaminergic pathophysiology and treatment.* Lancet Neurol, 2009. **8**(5): p. 464-74.
5. Halliday, G.M., et al., *Loss of brainstem serotonin- and substance P-containing neurons in Parkinson's disease.* Brain Res, 1990. **510**(1): p. 104-7.
6. Halliday, G.M., et al., *Neuropathology of immunohistochemically identified brainstem neurons in Parkinson's disease.* Ann Neurol, 1990. **27**(4): p. 373-85.
7. Gesi, M., et al., *The role of the locus coeruleus in the development of Parkinson's disease.* Neurosci Biobehav Rev, 2000. **24**(6): p. 655-68.
8. Zarow, C., et al., *Neuronal loss is greater in the locus coeruleus than nucleus basalis and substantia nigra in Alzheimer and Parkinson diseases.* Arch Neurol, 2003. **60**(3): p. 337-41.
9. Huang, K.W., et al., *Molecular and anatomical organization of the dorsal raphe nucleus.* Elife, 2019. **8**.
10. Pollak Dorocic, I., et al., *A whole-brain atlas of inputs to serotonergic neurons of the dorsal and median raphe nuclei.* Neuron, 2014. **83**(3): p. 663-78.
11. Soghomonian, J.J., L. Descarries, and K.C. Watkins, *Serotonin innervation in adult rat neostriatum. II. Ultrastructural features: a radioautographic and immunocytochemical study.* Brain Res, 1989. **481**(1): p. 67-86.
12. Maillet, A., et al., *Serotonergic and Dopaminergic Lesions Underlying Parkinsonian Neuropsychiatric Signs.* Mov Disord, 2021.
13. Jørgensen, L.M., et al., *Parkinson patients have a presynaptic serotonergic deficit: A dynamic deep brain stimulation PET study.* J Cereb Blood Flow Metab, 2021. **41**(8): p. 1954-1963.
14. Cheshire, P., et al., *Serotonergic markers in Parkinson's disease and levodopa-induced dyskinesias.* Mov Disord, 2015. **30**(6): p. 796-804.
15. Pifl, C., G. Schingnitz, and O. Hornykiewicz, *Effect of 1-methyl-4-phenyl-1,2,3,6-tetrahydropyridine on the regional distribution of brain monoamines in the rhesus monkey.* Neuroscience, 1991. **44**(3): p. 591-605.
16. Rylander, D., et al., *Maladaptive plasticity of serotonin axon terminals in levodopa-induced dyskinesia.* Ann Neurol, 2010. **68**(5): p. 619-28.
17. Nayyar, T., et al., *Cortical serotonin and norepinephrine denervation in parkinsonism: preferential loss of the beaded serotonin innervation.* Eur J Neurosci, 2009. **30**(2): p. 207-16.
18. Taylor, T.N., et al., *Nonmotor symptoms of Parkinson's disease revealed in an animal model with reduced monoamine storage capacity.* J Neurosci, 2009. **29**(25): p. 8103-13.

638 19. Karstaedt, P.J., et al., *Unilateral destruction of dopamine pathways increases ipsilateral*
639 *striatal serotonin turnover in rats.* Exp Neurol, 1994. **126**(1): p. 25-30.
640 20. Wilson, H., et al., *Serotonergic dysregulation is linked to sleep problems in Parkinson's*
641 *disease.* Neuroimage Clin, 2018. **18**: p. 630-637.
642 21. Politis, M., et al., *Depressive symptoms in PD correlate with higher 5-HTT binding in raphe*
643 *and limbic structures.* Neurology, 2010. **75**(21): p. 1920-7.
644 22. Kaya, A.H., et al., *Increased electrical and metabolic activity in the dorsal raphe nucleus of*
645 *Parkinsonian rats.* Brain Res, 2008. **1221**: p. 93-7.
646 23. Prinz, A., et al., *Increased excitability in serotonin neurons in the dorsal raphe nucleus in*
647 *the 6-OHDA mouse model of Parkinson's disease.* Exp Neurol, 2013. **248**: p. 236-45.
648 24. Guiard, B.P., et al., *Functional interactions between dopamine, serotonin and*
649 *norepinephrine neurons: an in-vivo electrophysiological study in rats with monoaminergic*
650 *lesions.* Int J Neuropsychopharmacol, 2008. **11**(5): p. 625-39.
651 25. Descarries, L., et al., *Dopaminergic projection from nucleus raphe dorsalis to neostriatum*
652 *in the rat.* J Comp Neurol, 1986. **249**(4): p. 511-20, 484-5.
653 26. Wenk, G.L., et al., *Behavioral, biochemical, histological, and electrophysiological effects*
654 *of 192 IgG-saporin injections into the basal forebrain of rats.* J Neurosci, 1994. **14**(10): p.
655 5986-95.
656 27. Lu, J., T.C. Jhou, and C.B. Saper, *Identification of wake-active dopaminergic neurons in the*
657 *ventral periaqueductal gray matter.* J Neurosci, 2006. **26**(1): p. 193-202.
658 28. Dzirasa, K., et al., *Dopaminergic control of sleep-wake states.* J Neurosci, 2006. **26**(41): p.
659 10577-89.
660 29. Cho, J.R., et al., *Dorsal Raphe Dopamine Neurons Modulate Arousal and Promote*
661 *Wakefulness by Salient Stimuli.* Neuron, 2017. **94**(6): p. 1205-1219.e8.
662 30. Lin, R., et al., *The Raphe Dopamine System Controls the Expression of Incentive Memory.*
663 Neuron, 2020. **106**(3): p. 498-514.e8.
664 31. Matthews, G.A., et al., *Dorsal Raphe Dopamine Neurons Represent the Experience of*
665 *Social Isolation.* Cell, 2016. **164**(4): p. 617-31.
666 32. Taylor, N.E., et al., *The Role of Glutamatergic and Dopaminergic Neurons in the*
667 *Periaqueductal Gray/Dorsal Raphe: Separating Analgesia and Anxiety.* eNeuro, 2019.
668 **6**(1).
669 33. Li, C., et al., *Mu Opioid Receptor Modulation of Dopamine Neurons in the Periaqueductal*
670 *Gray/Dorsal Raphe: A Role in Regulation of Pain.* Neuropsychopharmacology, 2016. **41**(8):
671 p. 2122-32.
672 34. Flores, J.A., et al., *Opiate anti-nociception is attenuated following lesion of large dopamine*
673 *neurons of the periaqueductal grey: critical role for D1 (not D2) dopamine receptors.* Pain,
674 2004. **110**(1-2): p. 205-14.
675 35. Flores, J.A., et al., *Role for dopamine neurons of the rostral linear nucleus and*
676 *periaqueductal gray in the rewarding and sensitizing properties of heroin.*
677 Neuropsychopharmacology, 2006. **31**(7): p. 1475-88.
678 36. Cardozo Pinto, D.F., et al., *Characterization of transgenic mouse models targeting*
679 *neuromodulatory systems reveals organizational principles of the dorsal raphe.* Nat
680 Commun, 2019. **10**(1): p. 4633.

681 37. Dougalis, A.G., et al., *Functional properties of dopamine neurons and co-expression of*
682 *vasoactive intestinal polypeptide in the dorsal raphe nucleus and ventro-lateral*
683 *periaqueductal grey.* Eur J Neurosci, 2012. **36**(10): p. 3322-3332.
684 38. Fu, W., et al., *Chemical neuroanatomy of the dorsal raphe nucleus and adjacent structures*
685 *of the mouse brain.* J Comp Neurol, 2010. **518**(17): p. 3464-94.
686 39. Okaty, B.W., et al., *Multi-Scale Molecular Deconstruction of the Serotonin Neuron System.*
687 Neuron, 2015. **88**(4): p. 774-91.
688 40. Lindeberg, J., et al., *Transgenic expression of Cre recombinase from the tyrosine*
689 *hydroxylase locus.* Genesis, 2004. **40**(2): p. 67-73.
690 41. Lammel, S., et al., *Diversity of transgenic mouse models for selective targeting of midbrain*
691 *dopamine neurons.* Neuron, 2015. **85**(2): p. 429-38.
692 42. Carter, M.E., et al., *Tuning arousal with optogenetic modulation of locus coeruleus*
693 *neurons.* Nat Neurosci, 2010. **13**(12): p. 1526-33.
694 43. Pudovkina, O.L., T.I. Cremers, and B.H. Westerink, *Regulation of the release of serotonin*
695 *in the dorsal raphe nucleus by alpha1 and alpha2 adrenoceptors.* Synapse, 2003. **50**(1): p.
696 77-82.
697 44. Trulson, M.E. and T. Crisp, *Role of norepinephrine in regulating the activity of serotonin-*
698 *containing dorsal raphe neurons.* Life Sci, 1984. **35**(5): p. 511-5.
699 45. Haddjeri, N., C. de Montigny, and P. Blier, *Modulation of the firing activity of*
700 *noradrenergic neurones in the rat locus coeruleus by the 5-hydroxtryptamine system.* Br J
701 Pharmacol, 1997. **120**(5): p. 865-75.
702 46. Singewald, N., et al., *Influence of excitatory amino acids on basal and sensory stimuli-*
703 *induced release of 5-HT in the locus coeruleus.* Br J Pharmacol, 1998. **123**(4): p. 746-52.
704 47. Aston-Jones, G., et al., *Serotonin selectively attenuates glutamate-evoked activation of*
705 *noradrenergic locus coeruleus neurons.* J Neurosci, 1991. **11**(3): p. 760-9.
706 48. Bonito-Oliva, A., D. Masini, and G. Fisone, *A mouse model of non-motor symptoms in*
707 *Parkinson's disease: focus on pharmacological interventions targeting affective*
708 *dysfunctions.* Front Behav Neurosci, 2014. **8**: p. 290.
709 49. Ztaou, S., et al., *Striatal cholinergic interneurons regulate cognitive and affective*
710 *dysfunction in partially dopamine-depleted mice.* Eur J Neurosci, 2018. **48**(9): p. 2988-
711 3004.
712 50. Bonito-Oliva, A., et al., *Cognitive impairment and dentate gyrus synaptic dysfunction in*
713 *experimental parkinsonism.* Biol Psychiatry, 2014. **75**(9): p. 701-10.
714 51. Poe, G.R., et al., *Locus coeruleus: a new look at the blue spot.* Nat Rev Neurosci, 2020.
715 **21**(11): p. 644-659.
716 52. Szot, P., et al., *Lesioning noradrenergic neurons of the locus coeruleus in C57Bl/6 mice*
717 *with unilateral 6-hydroxydopamine injection, to assess molecular, electrophysiological*
718 *and biochemical changes in noradrenergic signaling.* Neuroscience, 2012. **216**: p. 143-57.
719 53. Neuhoff, H., et al., *I(h) channels contribute to the different functional properties of*
720 *identified dopaminergic subpopulations in the midbrain.* J Neurosci, 2002. **22**(4): p. 1290-
721 302.
722 54. Lammel, S., et al., *Unique properties of mesoprefrontal neurons within a dual*
723 *mesocorticolimbic dopamine system.* Neuron, 2008. **57**(5): p. 760-73.

55. Strickland, J.A. and M.A. McDannald, *Brainstem networks construct threat probability and prediction error from neuronal building blocks.* Nat Commun, 2022. **13**(1): p. 6192.
56. Hajós, M., et al., *Neurochemical identification of stereotypic burst-firing neurons in the rat dorsal raphe nucleus using juxtacellular labelling methods.* Eur J Neurosci, 2007. **25**(1): p. 119-26.
57. Schweimer, J.V., et al., *Spike-timing relationship of neurochemically-identified dorsal raphe neurons during cortical slow oscillations.* Neuroscience, 2011. **196**(4): p. 115-23.
58. Dahlstroem, A. and K. Fuxe, *EVIDENCE FOR THE EXISTENCE OF MONOAMINE-CONTAINING NEURONS IN THE CENTRAL NERVOUS SYSTEM. I. DEMONSTRATION OF MONOAMINES IN THE CELL BODIES OF BRAIN STEM NEURONS.* Acta Physiol Scand Suppl, 1964: p. Suppl 232:1-55.
59. Weissbourd, B., et al., *Presynaptic partners of dorsal raphe serotonergic and GABAergic neurons.* Neuron, 2014. **83**(3): p. 645-62.
60. Gocho, Y., et al., *Electrophysiological and pharmacological properties of GABAergic cells in the dorsal raphe nucleus.* J Physiol Sci, 2013. **63**(2): p. 147-54.
61. Xu, Z., et al., *Whole-brain connectivity atlas of glutamatergic and GABAergic neurons in the mouse dorsal and median raphe nuclei.* Elife, 2021. **10**.
62. Bowker, R.M., et al., *Descending serotonergic, peptidergic and cholinergic pathways from the raphe nuclei: a multiple transmitter complex.* Brain Res, 1983. **288**(1-2): p. 33-48.
63. Rivera, H.M. and C.L. Bethea, *Ovarian steroids increase PSD-95 expression and dendritic spines in the dorsal raphe of ovariectomized macaques.* Synapse, 2013. **67**(12): p. 897-908.
64. Park, M.R., *Intracellular horseradish peroxidase labeling of rapidly firing dorsal raphe projection neurons.* Brain Res, 1987. **402**(1): p. 117-30.
65. Calizo, L.H., et al., *Raphe serotonin neurons are not homogenous: electrophysiological, morphological and neurochemical evidence.* Neuropharmacology, 2011. **61**(3): p. 524-43.
66. Diaz-Cintra, S., et al., *Nucleus raphe dorsalis: a morphometric Golgi study in rats of three age groups.* Brain Res, 1981. **207**(1): p. 1-16.
67. Li, Y.Q., et al., *Morphological features and electrophysiological properties of serotonergic and non-serotonergic projection neurons in the dorsal raphe nucleus. An intracellular recording and labeling study in rat brain slices.* Brain Res, 2001. **900**(1): p. 110-8.
68. Kamińska, K., et al., *Depressive-like neurochemical and behavioral markers of Parkinson's disease after 6-OHDA administered unilaterally to the rat medial forebrain bundle.* Pharmacol Rep, 2017. **69**(5): p. 985-994.
69. Fulceri, F., et al., *Nigrostriatal damage with 6-OHDA: validation of routinely applied procedures.* Ann N Y Acad Sci, 2006. **1074**: p. 344-8.
70. Wang, S., et al., *Unilateral lesion of the nigrostriatal pathway induces an increase of neuronal firing of the midbrain raphe nuclei 5-HT neurons and a decrease of their response to 5-HT(1A) receptor stimulation in the rat.* Neuroscience, 2009. **159**(2): p. 850-61.
71. Masini, D., et al., *A Guide to the Generation of a 6-Hydroxydopamine Mouse Model of Parkinson's Disease for the Study of Non-Motor Symptoms.* Biomedicines, 2021. **9**(6).
72. Feng, L., T. Zhao, and J. Kim, *neuTube 1.0: A New Design for Efficient Neuron Reconstruction Software Based on the SWC Format.* eNeuro, 2015. **2**(1).

73. Hjorth, J.J.J., et al., *The microcircuits of striatum in silico.* Proc Natl Acad Sci U S A, 2020. **117**(17): p. 9554-9565.

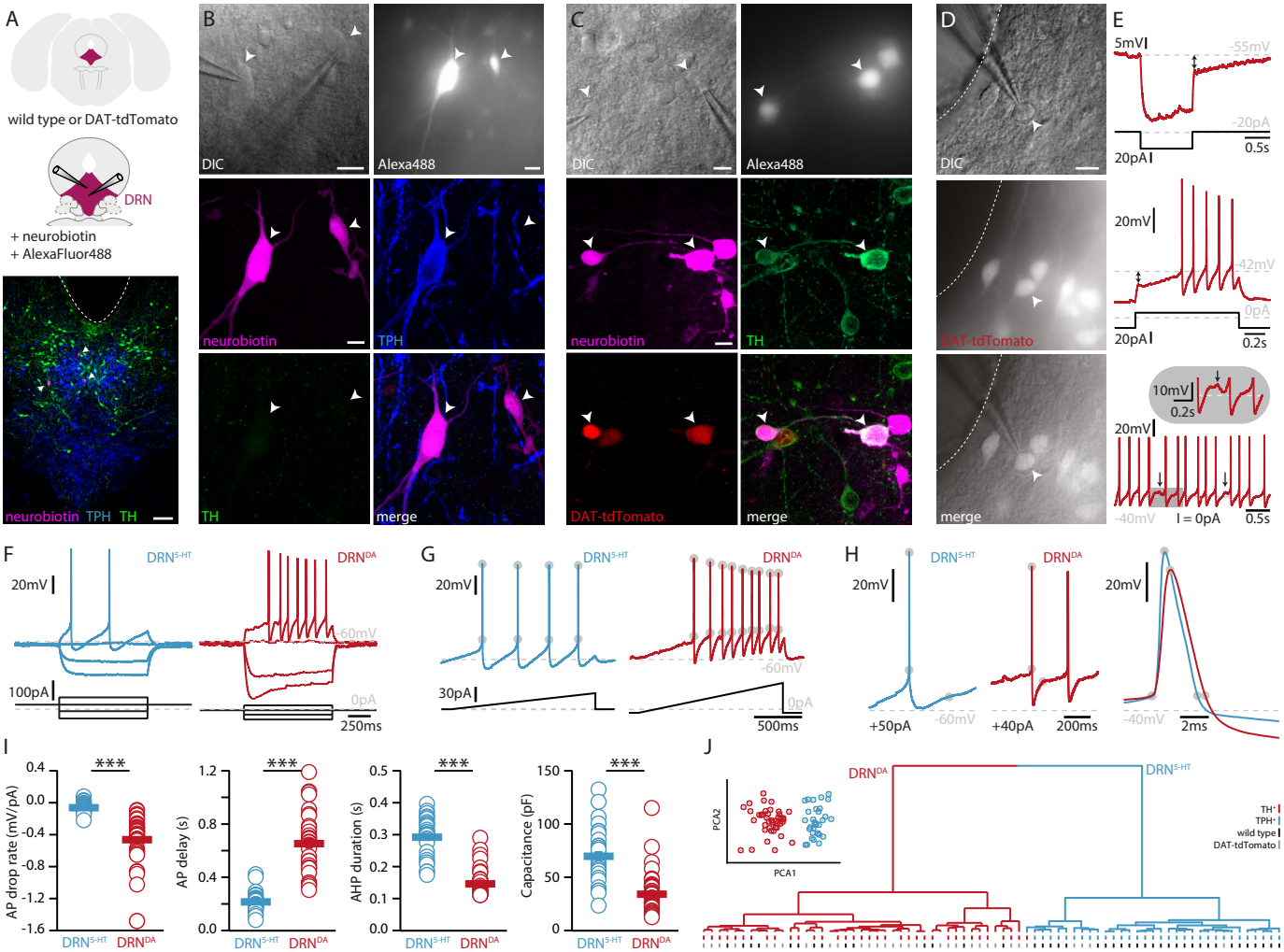
A
wild type or DAT-tdTomato
DRN
+ neurobiotin
+ AlexaFluor488
neurobiotin TPH TH
B
DIC
Alexa488
neurobiotin
TPH
TH
merge
C
DIC
Alexa488
neurobiotin
TH
DAT-tdTomato
merge
D
DIC
DAT-tdTomato
merge
E
5mV
-55mV
-20pA
20pA
0.5s
20mV
-42mV
0pA
20pA
0.2s
10mV
0.2s
20mV
-40mV
I = 0pA
0.5s
F
DRN5-HT
DRNDA
20mV
100pA
-60mV
0pA
250ms
G
DRN5-HT
DRNDA
20mV
30pA
-60mV
0pA
500ms
H
DRN5-HT
DRNDA
20mV
+50pA
-60mV
+40pA
200ms
-40mV
2ms
I
AP drop rate (mV/pA)
AP delay (s)
AHP duration (s)
Capacitance (pF)
***
DRN5-HT
DRNDA
J
DRNDA
DRN5-HT
PCA2
PCA1
TH+
TPH+
wild type
DAT-tdTomato

Fig. 1

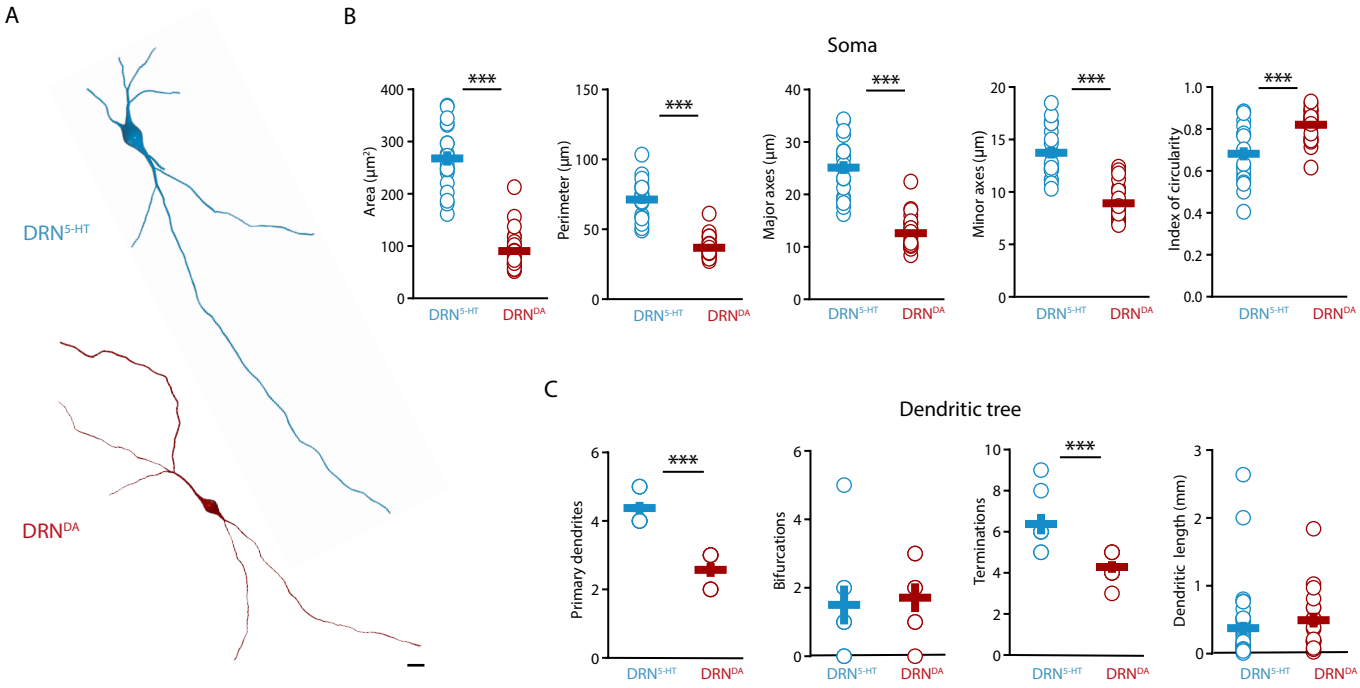
A
DRN5-HT
DRNDA
B
Soma
Area (µm²)
Perimeter (µm)
Major axes (µm)
Minor axes (µm)
Index of circularity
***
DRN5-HT
DRNDA
C
Dendritic tree
Primary dendrites
Bifurcations
Terminations
Dendritic length (mm)

Fig. 2

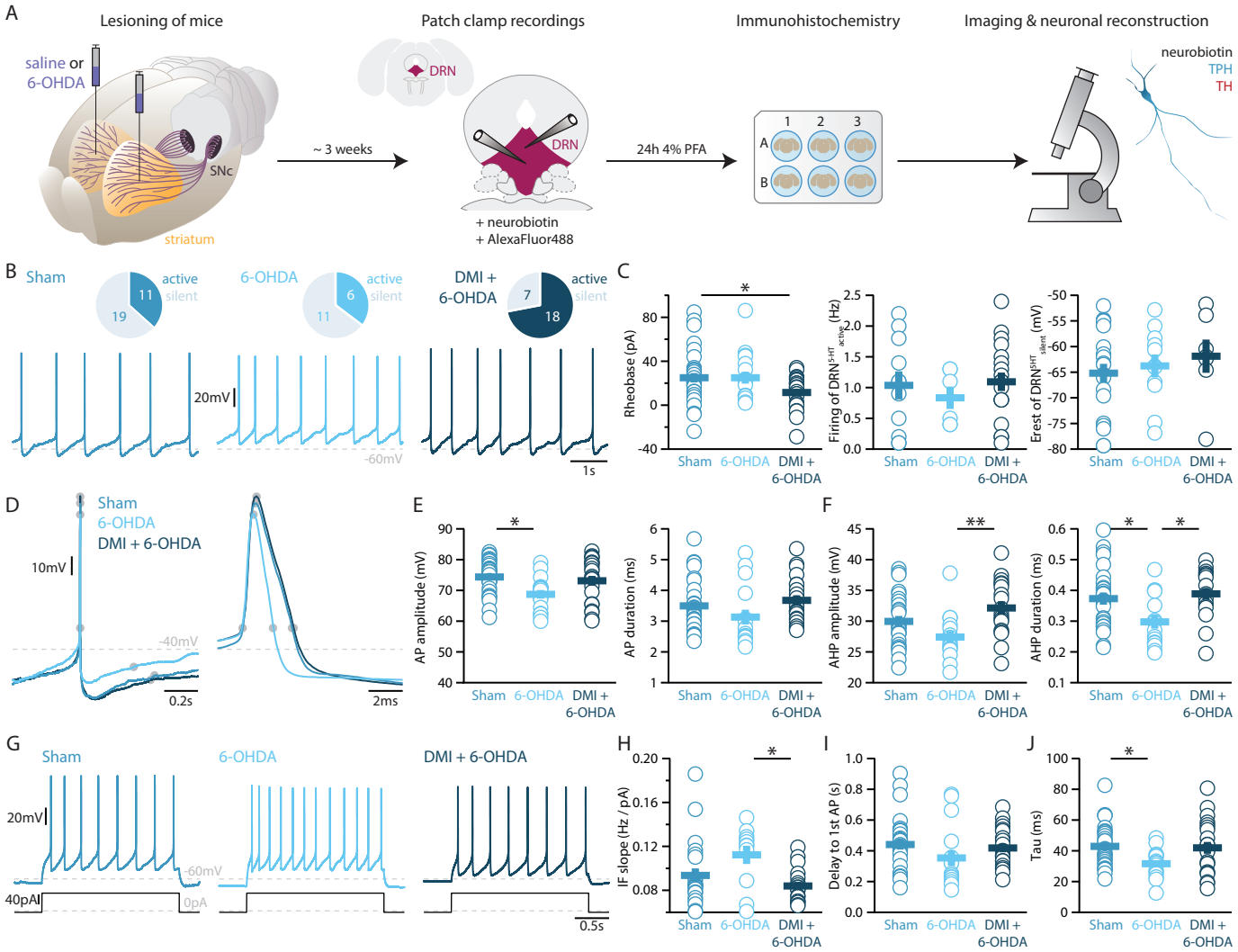
A
Lesioning of mice
Patch clamp recordings
Immunohistochemistry
Imaging & neuronal reconstruction
saline or
6-OHDA
SNc
striatum
~ 3 weeks
DRN
+ neurobiotin
+ AlexaFluor488
24h 4% PFA
1
2
3
A
B
neurobiotin
TPH
TH
B
Sham
active
silent
11
19
6-OHDA
6
11
DMI +
6-OHDA
7
18
20mV
-60mV
1s
C
Rheobase (pA)
Firing of DRN5-HT active (Hz)
Erest of DRN5-HT silent (mV)
Sham
6-OHDA
DMI +
6-OHDA
D
Sham
6-OHDA
DMI + 6-OHDA
10mV
-40mV
0.2s
2ms
E
AP amplitude (mV)
AP duration (ms)
F
AHP amplitude (mV)
AHP duration (ms)
G
Sham
6-OHDA
DMI + 6-OHDA
20mV
-60mV
40pA
0pA
0.5s
H
IF slope (Hz / pA)
I
Delay to 1st AP (s)
J
Tau (ms)

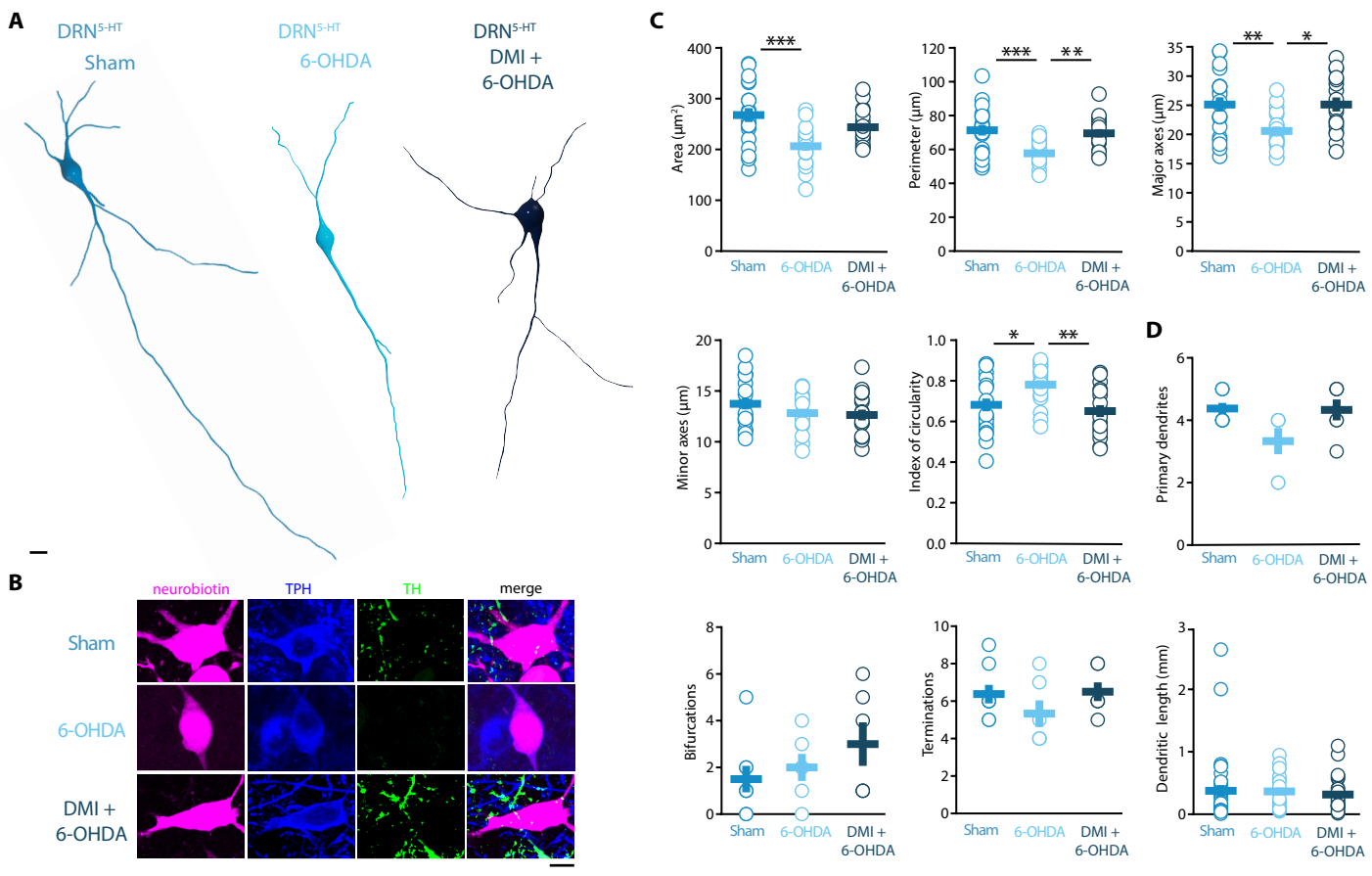
A
DRN5-HT
Sham
DRN5-HT
6-OHDA
DRN5-HT
DMI +
6-OHDA
B
neurobiotin
TPH
TH
merge
Sham
6-OHDA
DMI +
6-OHDA
C
Area (µm²)
Perimeter (µm)
Major axes (µm)
Minor axes (µm)
Index of circularity
Bifurcations
Terminations
Dendritic length (mm)
Sham
6-OHDA
DMI +
6-OHDA
D
Primary dendrites

Fig. 4

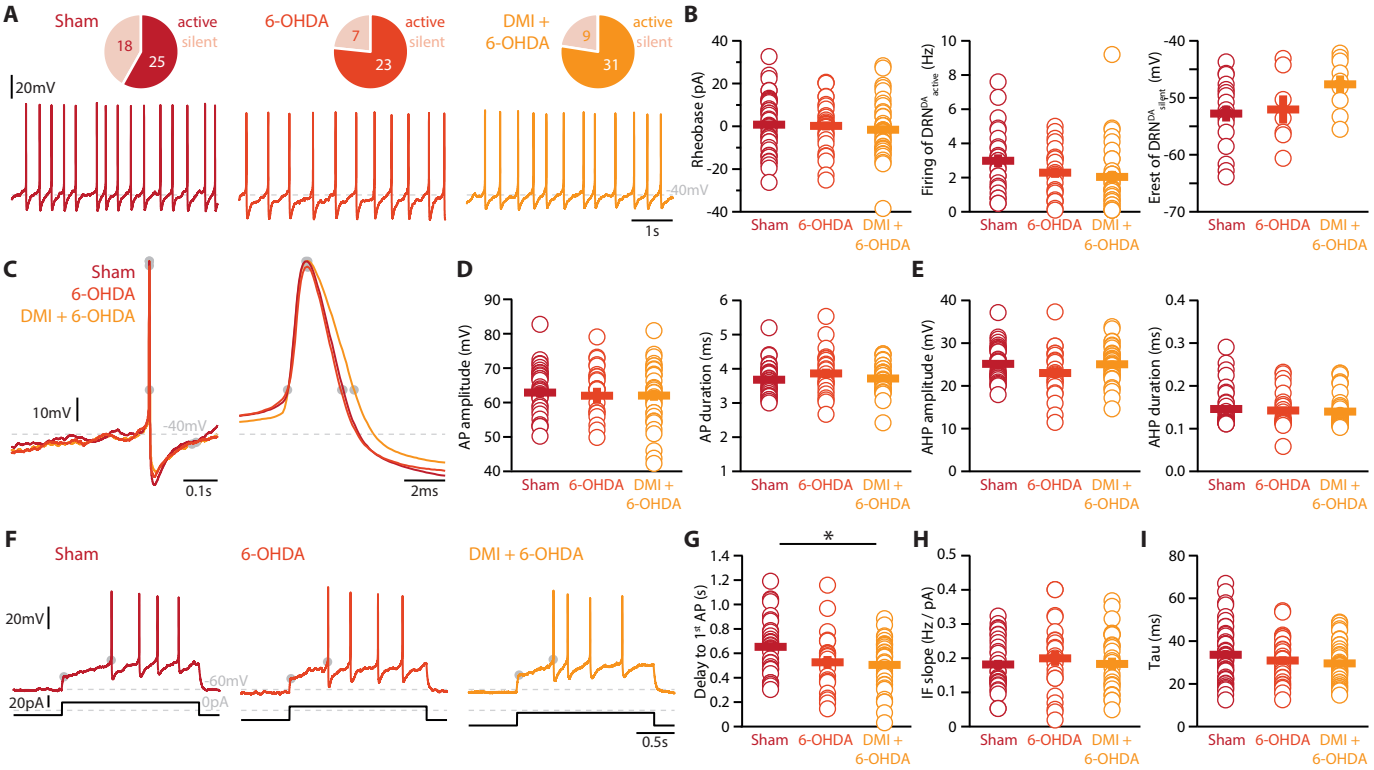
A
Sham
active
silent
18
25
6-OHDA
7
23
DMI + 6-OHDA
9
31
20mV
-40mV
1s
B
Rheobase (pA)
Firing of DRN^DA active (Hz)
Erest of DRN^DA silent (mV)
Sham
6-OHDA
DMI + 6-OHDA
C
Sham
6-OHDA
DMI + 6-OHDA
10mV
-40mV
0.1s
2ms
D
AP amplitude (mV)
AP duration (ms)
E
AHP amplitude (mV)
AHP duration (ms)
F
Sham
6-OHDA
DMI + 6-OHDA
20mV
-60mV
20pA
0pA
0.5s
G
*
Delay to 1st AP (s)
H
IF slope (Hz / pA)
I
Tau (ms)

Fig. 5

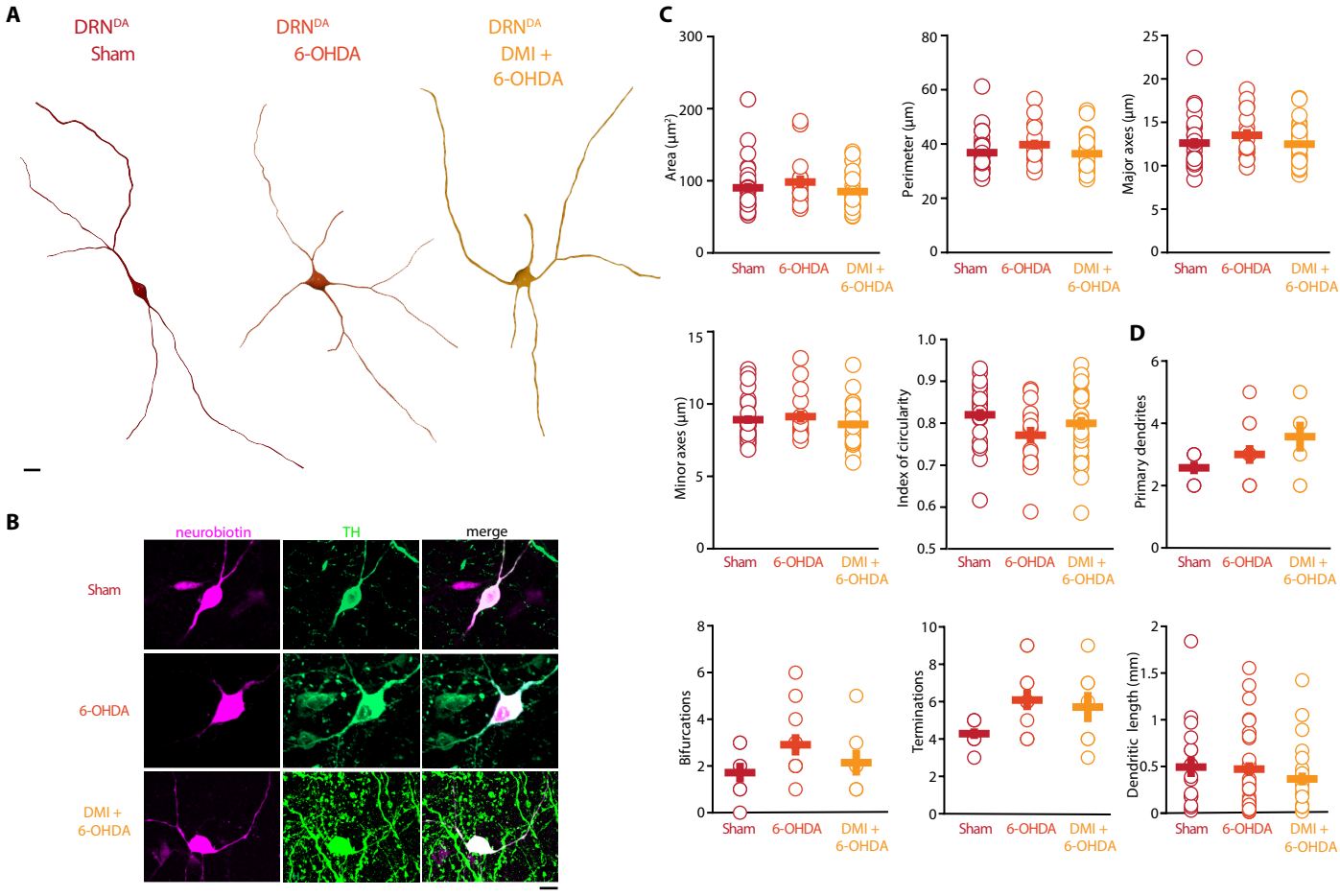
A
DRN^DA
Sham
DRN^DA
6-OHDA
DRN^DA
DMI +
6-OHDA
B
neurobiotin
TH
merge
Sham
6-OHDA
DMI +
6-OHDA
C
Area (µm²)
Perimeter (µm)
Major axes (µm)
Minor axes (µm)
Index of circularity
Primary dendrites
Bifurcations
Terminations
Dendritic length (mm)
Sham
6-OHDA
DMI +
6-OHDA
D

Fig. 6